PHYSICAL REVIEW FLUIDS **1**, 051901(R) (2016)

Size of the top jet drop produced by bubble bursting

Elisabeth Ghabache and Thomas Séon*

Sorbonne Universités, Université Pierre et Marie Curie, and Centre National de la Recherche Scientifique, Unité Mixte de Recherche No. 7190, Institut Jean Le Rond d'Alembert, 4 Place Jussieu, F-75005 Paris, France

(Received 10 May 2016; published 13 September 2016)

As a bubble bursts at a liquid-air interface, a tiny liquid jet rises and can release the so-called jet drops. In this paper the size of the top jet drop produced by a bubble bursting is investigated experimentally. We determine and discuss the first scaling law enabling the determination of the top jet drop size as a function of the corresponding mother bubble radius and the liquid properties (viscosity, surface tension, and density), along with its regime of existence. Furthermore, with the aim of decoupling experimentally the effects of bubble collapse and jet dynamics on the drop detachment, we propose a scaling providing the top drop size only as a function of the jet velocity and liquid parameters. In particular, this allows us to untangle the intricate roles of viscosity, gravity, and surface tension in the end pinching of the bubble bursting jet.

DOI: 10.1103/PhysRevFluids.1.051901

After a bubble rises in the ocean, it reaches the surface and the thin film that separates the bubble from the atmosphere, the bubble cap, drains and ruptures under the effect of gravity [1]. From then, two events in a row produce droplets: the film shattering, which expels on the order of 10–100 small film drops [2], and the capillary collapse of the remaining cavity, which shoots up a central jet, which becomes unstable and breaks up into several larger jet drops [3]. Most film drops are less than 1 μm in radius, while jet drops span a range from 2 to 500 μm [4]. Sea spray is largely attributed to an estimated 10^{18}–10^{20} bubbles that burst every second across the oceans [5]. The main consequences of this aerosol are a global emission of about 10^{12}–10^{14} kg per year of sea salt and heat and momentum transfer with the atmosphere through direct exchange [1].

On a smaller scale, the situation found in glasses of champagne and sparkling wines is comparable, except for a major difference: The liquid properties of a hydroalcoholic solution are different in that the surface tension is lower ($\gamma = 48$ mN m^{-1}) and the liquid viscosity ranges from $\mu = 1.6$ to 3.6 mPa s as champagne temperature changes during tasting [6]. Subsequent consequences of these different properties include almost no film drops being produced above a glass of champagne and the dynamics of jet drops is strongly modified by liquid parameters [7]. Furthermore, we showed in a recent study [8] that the top jet drops, which bound the edge of the aerosol cloud, dominate the evaporation process as they are faster and usually bigger than the others or of comparable size. In this paper the size of the top jet drop produced by bubble bursting is investigated as a function of the mother bubble size [9] and the liquid properties (see Fig. 1).

An infinite cylinder of liquid at rest, subjected to the influence of surface tension, will break up into a number of individual droplets through the so-called Rayleigh-Plateau instability. The bubble bursting jets, depicted in Fig. 1, are finite and do not break as a consequence of Rayleigh-Plateau instability. Instead, the breakup takes place at the jet tip and detaches one drop at a time. This mechanism, called end pinching, consists of a competition between the capillary retraction of the jet tip, shaping a blob [10], and a pressure-driven flow from the cylindrical jet toward the bulbous end. This leads to the development of a neck, where the jet joins the blob, and thus to the drop detachment via a capillary pinch-off process. This mechanism was first described in the context of a strongly deformed viscous drop [11] and later for a free liquid filament of arbitrary viscosity [12]. This

*Corresponding author: thomas.seon@gmail.com

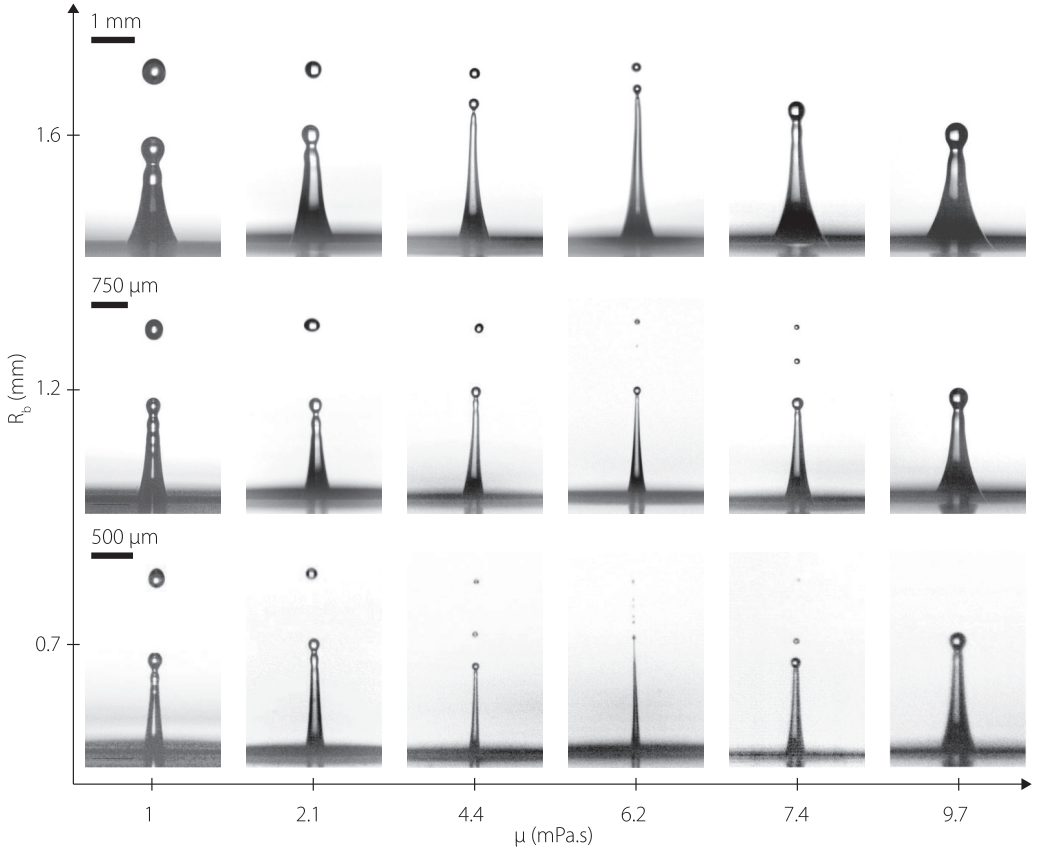

FIG. 1. Snapshot of a typical jetting event following a bubble bursting at a free surface. The shapes of the jets and drops are displayed for three mother bubble radii, reported on the y axis, bursting in water and five water-glycerol mixtures of viscosity indicated on the x axis. For those six solutions, the surface tension is almost constant (ranging from 64 to 72 mN m^{-1}), so one mainly observes in this figure the effect of changing viscosity. The top drop size decreases with bubble radius and increasing liquid viscosity. The biggest drop, on the top left corner of this diagram, has a radius of about 400 μm and the smallest ($R_b = 0.7$ mm and $\mu = 7.4$ mPa s) reaches 20 μm. The scale bar is showed on the top left corner of each bubble radius and is the same for the whole row.

end-pinching capillary breakup of liquid jets is important in several industrial contexts, especially because of the broad range of applications of inkjet printing technology. Indeed, it enables accurate drop deposition of liquids and includes the production of organic thin-film transistors, liquid crystal displays, fuel or solar cells, printed circuit boards, dispensing of DNA and protein substances, or even fabrication of living tissue [13]. Recently, the end-pinching of a stretched inertially driven jet shooting up after a cavity collapse was described theoretically and numerically [14]. These stretched jets are found in many situations [15,16], in particular bubble bursting, and they all have similar properties.

Our paper aims thus at contributing to the understanding and characterizing of the end-pinching of such stretched jets. This will be realized through the experimental characterization of the size of the top jet drop and its variations with respect to its natural control parameters, when a jet droplet is produced by a single bubble bursting at a calm liquid surface. Scaling laws of the drop diameter along with their regime of existence will be determined and discussed.

γ (mN/m)	72	67	65	65	65	64	64	48	48	48
μ (mPa s)	1.0	2.1	3.3	4.4	5.2	6.2	7.4	1.6	2.6	3.6

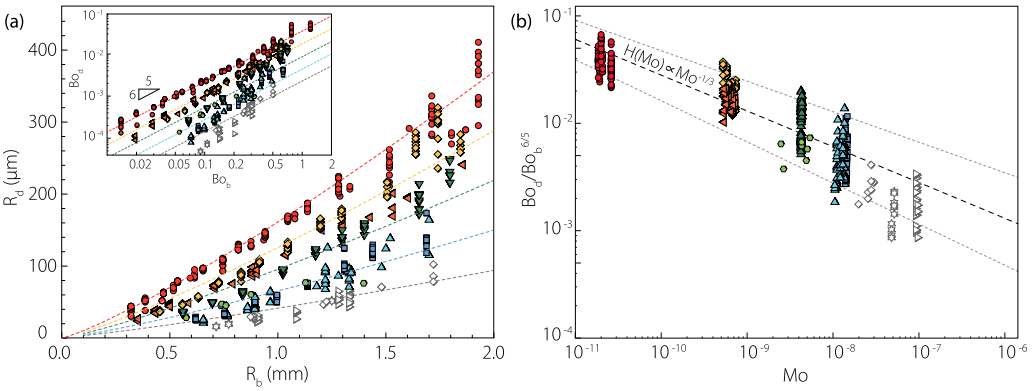

FIG. 2. (a) Top drop radius as a function of the mother bubble radius for bubble bursting in liquids with different surface tension and viscosity. The parameters of these liquids associated with the corresponding symbols are summarized in the table above the graph. In the inset, the Bond number built on the drop radius is plotted as a function of the Bond number built on the bubble radius for the same liquids. The dashed lines represent $R_d \propto R_b^{6/5}$ in the graph and $\mathrm{Bo}_d \propto \mathrm{Bo}_b^{6/5}$ in the inset. (b) $\mathrm{Bo}_d/\mathrm{Bo}_b^{6/5}$ as a function of the Morton number. The dashed line fits the experimental data plotted with closed symbols, up to $\mathrm{Mo} \sim 10^{-8}$, following the trend $\mathrm{Bo}_d/\mathrm{Bo}_b^{6/5} \propto \mathrm{Mo}^{-1/3}$. The error bar on the exponent is $1/20$ and the two bounds $H(\mathrm{Mo}) \propto \mathrm{Mo}^{-1/3\pm1/20}$ are plotted on the graph with a dotted line.

The experiment consists in releasing a gas bubble from a submerged needle in a liquid and recording the upward jet and released drops after the bubble bursts at the free surface. Different needle diameters allow us to create bubbles with various radii R_b ranging from 0.3 to 2 mm. The liquids used include 11 solutions of water-glycerol-ethanol mixtures of viscosity in the range $\mu = 1$–9.7 mPa s, surface tension $\gamma = 48$–72 mN m^{-1}, and density $\rho = 980$–1140 kg m^{-3}. The surface tension and viscosity of each solution is presented along with the corresponding symbol in the table at the top of Fig. 2. The jet dynamics is analyzed through extreme close-up ultrafast imagery, using a digital high-speed camera (Photron SA-5). Macrolenses and extension rings allow us to record with a definition reaching 5 μm per pixel.

Figure 1 presents the jet and released drop shape following bubble bursting. In the cases where no drop detaches, the jets are displayed at their maximum height. On the x and y axes the jet and drop shapes are represented, respectively, for six different liquid viscosities and three different mother bubble radii. It is clear on this diagram that, independently of the viscosity, the bigger the bubble, the bigger the top drop. This intuitive result has been observed in water in various previous studies [9]. Although mentioned in a earlier paper [3], the variation with viscosity is much more unexpected. Indeed, irrespectively of the bubble radius in the range considered here, the top drop shrinks as viscosity is increased and seems to reach a minimum for a liquid viscosity around 6–7 mPa s here. For higher viscosities, no drop is detached, in accordance with a previous study [17]. This decrease of the drop radius with viscosity is surprising, in particular because the Ohnesorge number based on the drop radius, namely, $\mathrm{Oh} = \mu/\sqrt{\rho R_d \gamma}$, which compares the effect of viscosity and capillarity, is included between 10^{-1} and 10^{-3} and is consequently always lower than 1. This therefore suggests that viscous effects should be neglected in the description of jet breakup, as done in similar cases [14]. We will see further why, in this particular case of bubble bursting jet, the liquid viscosity has such a strong influence.

We now plot, in Fig. 2(a), the variation of the top drop radius R_d as a function of the mother bubble radius R_b for different values of the liquid parameters (μ, γ, and ρ) indicated in the table

above. This quantifies our previous observation of drop shrinking with decreasing bubble radius and increasing liquid viscosity, from 400 to 20 μm for the solutions plotted here. We also observe that the same drop shrinking occurs when surface tension is decreased. Moreover, it appears that, regardless of the liquid parameters considered in this graph, the drop size increases with bubble radius following roughly the same variation for all the curves, $R_d \propto R_b^{6/5}$, shown with dashed lines on the graph. Note that the historical law, proposed for the top jet drop radius produced by bubble bursting in water, which predicts a drop radius being one-tenth of the bubble radius ($R_d = R_b/10$) [18], is only valid for bubble radii smaller than 500 μm. More accurate laws have been written ever since. In particular, when $R_b \geqslant 0.1$ mm, the relationship $R_d = 0.075 R_b^{1.3}$ has been proposed, with radii expressed in millimeters [19]. This variation is very closed to the one we find.

Because of the experimental relationship between R_d and R_b, we are now able to write a more universal scaling law, taking into account the liquid parameters. It is clear that the top drop size depends on the bubble radius R_b and liquid viscosity μ and we assume that the surface tension γ, density ρ, and gravity g might also influence its selection, yielding

$$R_d = \Pi(R_b, \rho, \mu, \gamma, g).$$

Using dimensional arguments, this equation becomes a relation between three dimensionless numbers fully describing the top drop size selection

$$\mathrm{Bo}_d = F(\mathrm{Bo}_b, \mathrm{Mo}),$$

where the Bond numbers $\mathrm{Bo}_d = \rho g R_d^2/\gamma$ and $\mathrm{Bo}_b = \rho g R_b^2/\gamma$ compare the effect of gravity and capillarity on the top drop and the initial bubble, respectively, and the Morton number $\mathrm{Mo} = g\mu^4/\rho\gamma^3$ only depends on the fluid properties and is, in particular, independent of the bubble radius R_b. In the inset of Fig. 2(a) the variation of the top drop Bond number is plotted as a function of the mother bubble Bond number for the same solutions as in Fig. 2(a). The variation $\mathrm{Bo}_d \propto \mathrm{Bo}_b^{6/5}$ is also plotted with dashed lines. This power law, independent of the liquid parameters, still works reasonably well, allowing us to write the scaling law

$$\mathrm{Bo}_d = \mathrm{Bo}_b^{6/5} H(\mathrm{Mo}). \tag{1}$$

With the aim of estimating the dependence of the drop size with the liquid properties, namely, $H(\mathrm{Mo})$, $\mathrm{Bo}_d/\mathrm{Bo}_b^{6/5}$ is plotted as a function of the Morton number in Fig. 2(b). We observe that the data with closed symbols gather along a line, up to $\mathrm{Mo} \simeq 10^{-8}$, corresponding to a viscosity $\mu = 5.2$ mPa s for a water-glycerol mixture. This line is properly fitted by $H(\mathrm{Mo}) = \mathcal{A}\mathrm{Mo}^{-1/3}$ with $\mathcal{A} = 1.1 \times 10^{-5}$. As the results are slightly scattered, we estimate the error bar by fitting the lower and upper bounds and we find $H(\mathrm{Mo}) \propto \mathrm{Mo}^{-1/3\pm1/20}$; these two bounds are plotted on the graph with a dotted line. Therefore, in this regime, ranging around three decades for the Morton number, we establish a scaling law for the top drop size as a function of the bubble radius and liquid parameters, in the context of bubble bursting

$$\mathrm{Bo}_d = \mathcal{A}\mathrm{Bo}_b^{6/5}\mathrm{Mo}^{-1/3}. \tag{2}$$

This result is essential because the bubble radius and the liquid parameters are the natural experimental parameters for a bursting bubble aerosol measurement. In particular, the size distribution of bubbles is know in the ocean [20] and can even be controlled in a glass of champagne [21].

However, under this form, Eq. (2) is difficult to interpret, in particular, the confusing role of viscosity, which is expected to be negligible ($\mathrm{Oh} \ll 1$). In addition, this scaling law contains substantial experimental data scattering due to an accumulation of variability, when the jet is created and when the drop is detached. Therefore, in the following we want to express the drop radius as a function of only jet parameters, typically by disposing of the bubble radius.

When a bubble collapses, a jet is formed with a given shape, tip velocity, local strain rate, etc. In this regime, where $\mathrm{Mo} \lesssim 10^{-8}$, the decrease of the drop size with Morton number is accompanied by

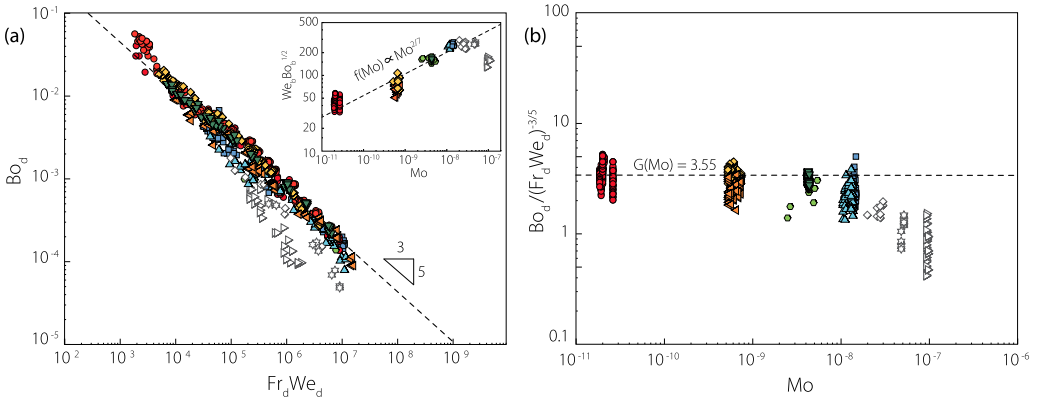

FIG. 3. (a) Drop Bond number as a function of the product of the Froud and Weber numbers $\mathrm{Fr}_d\mathrm{We}_d = \rho V_{\mathrm{tip}}^4/\gamma g$ for various values of the Morton number. For $\mathrm{Mo} \lesssim 10^{-8}$, all the data, plotted with closed symbols, collapse on a single curve following the trend $\mathrm{Bo}_d = \mathcal{C}(\mathrm{Fr}_d\mathrm{We}_d)^{-3/5}$ as shown by the dashed line. In the inset, Fig. 3(b) of Ref. [3] is plotted in a log-log plot; $f(\mathrm{Mo}) = \mathcal{B}\mathrm{Mo}^{2/7}$ fits reasonably well the data for $\mathrm{Mo} \in [10^{-11}, 10^{-8}]$, as shown by the dashed line. (b) $\mathrm{Bo}_d/(\mathrm{Fr}_d\mathrm{We}_d)^{-3/5}$ as a function of Morton number. The dashed line fitting the data on the same range is a constant equal to $\mathcal{C}$. Data corresponding to $\mathrm{Mo} \in [10^{-8}, 10^{-7}]$, plotted with open symbols, leave the inviscid regime. Above $\mathrm{Mo} \simeq 10^{-7}$ no more drops can detach.

a thinning down of the whole jet and an increase of the jet velocity. This has been largely discussed in a previous study [3] and the corresponding scaling law, for the jet velocity as a function of the bubble radius and liquid parameters, has been proposed: $\mathrm{We}_b = \mathrm{Bo}_b^{-1/2} f(\mathrm{Mo})$, where the Weber number $\mathrm{We}_b = \rho V_{\mathrm{tip}}^2 R_b/\gamma$ compares the effect of inertia and capillarity on the jet dynamics, V_{tip} being the jet tip velocity as the jet passes the free surface level. Therefore, with the aim of decoupling the effects of bubble collapse and jet dynamics on the drop detachment, $\mathrm{We}_b = \mathrm{Bo}_b^{-1/2} f(\mathrm{Mo})$ is combined with Eq. (2) to eliminate the bubble radius. This eventually yields the following scaling law relating the drop radius, the jet velocity, and the liquid parameters:

$$\mathrm{Bo}_d = (\mathrm{Fr}_d\mathrm{We}_d)^{-3/5} G(\mathrm{Mo}), \tag{3}$$

where $\mathrm{Fr}_d = V_{\mathrm{tip}}^2/gR_d$, leading to $\mathrm{Fr}_d\mathrm{We}_d = \rho V_{\mathrm{tip}}^4/\gamma g$, which compares the effect of inertia upon capillarity and gravity on the jet dynamics and is, in particular, independent of bubble radius and viscosity. In order to estimate $G(\mathrm{Mo}) = H(\mathrm{Mo}) f(\mathrm{Mo})^{6/5}$, $f(\mathrm{Mo})$ needs to be known. In the inset of Fig. 3, $\mathrm{We}_b\mathrm{Bo}_b^{1/2}$ is plotted as a function of Mo [Fig. 3(b) of Ref. [3]] on a log-log plot allowing us to determine $f(\mathrm{Mo})$ by fitting the data in the same regime ($10^{-11} \lesssim \mathrm{Mo} \lesssim 10^{-8}$). The power law $f(\mathrm{Mo}) = \mathcal{B}\mathrm{Mo}^{2/7}$, with $\mathcal{B} = 3.9 \times 10^4$, fits reasonably well the experimental data. Consequently, $G(\mathrm{Mo}) = \mathcal{A}\mathrm{Mo}^{-1/3}(\mathcal{B}\mathrm{Mo}^{2/7})^{6/5} = \mathcal{C}\mathrm{Mo}^{1/105} \sim \mathcal{C}$, with $\mathcal{C} = \mathcal{A}\mathcal{B}^{6/5} = 3.55$. This signifies that viscosity is removed from the scaling law relating the drop radius, the jet velocity, and the liquid parameters, leading to, for $\mathrm{Mo} \lesssim 10^{-8}$,

$$\mathrm{Bo}_d = \mathcal{C}(\mathrm{Fr}_d\mathrm{We}_d)^{-3/5}. \tag{4}$$

In Fig. 3(a) the drop Bond number Bo_d is therefore plotted as a function of $\mathrm{Fr}_d\mathrm{We}_d$ and we observe an excellent collapse of all the experimental data represented with closed symbols, confirming Eq. (4). Figure 3(b) presents $\mathrm{Bo}_d/(\mathrm{Fr}_d\mathrm{We}_d)^{-3/5}$ as a function of Morton number and confirms that the drop Bond number is independent of viscosity for the closed symbols. This inviscid behavior stops at $\mathrm{Mo} \simeq 10^{-8}$, viscosity playing a role for data represented by open symbols, between 10^{-8} and 10^{-7} (corresponding to $\mu \sim 5$ and 7 mPa s for water-glycerol mixtures). Above $\mathrm{Mo} \simeq 10^{-7}$ no more drops can detach.

Equation (4), valid for Mo $\lesssim 10^{-8}$, is therefore the more robust, with less scattering than Eq. (2). Furthermore, it demonstrates that viscosity does not participate in the drop detachment process. This result was predictable as the Ohnesorge number is always lower than one. However, we may now wonder why the drop radius was dependent on the liquid viscosity in Figs. 1 and 2 and Eq. (2). Actually, this influence of viscosity on drop size was only through the jet's formation as a memory of the bubble collapse. Indeed, as a bubble collapses, capillary waves focus at the bottom of the cavity giving birth to the jet. Increasing the liquid viscosity changes the wave focusing, producing a thinner jet (see Ref. [3] for details) and therefore smaller droplets. In Eq. (4) this shaping effect is then entirely contained through V_{tip} and viscosity can disappear, shedding light on the inviscid behavior of the drop detachment mechanism. Finally, the Bond number of the drop seems to be only selected by a competition between the given inertia, which makes the jet rising and stretching, and the duet gravity-capillarity that pulls on the jet tip so as to form a blob, initiating an end-pinching mechanism and consequently releasing a drop. While the influence of capillarity is obvious in this blob formation, the one of gravity can be more surprising. However, at the height the drop is detached, the gravity can already play a role. Indeed, the Froude number built on the drop detachment height h_{det}, $\text{Fr}h_{\text{det}} = V_{\text{tip}}^2/gh_{\text{det}}$, is of $O(1)$ for top drops projected by the largest bubbles.

As a conclusion we provide experimentally two different scaling laws giving the top jet drop radius ejected after a bubble burst as a function of the liquid parameters and the mother bubble radius in Eq. (2) or the jet velocity in Eq. (4). These results induce various outcomes. The size distribution of the top jet drop aerosol can now easily be computed as long as we know the bubble size distribution, which is the case in oceans, for example [20]. Note that the top jet drop plays a crucial role in terms of chemical exchange and evaporation, as it is usually bigger and faster than the followers [7]. These results also apply to slightly viscous liquids (up to Mo $\sim 10^{-8}$) like champagne or sparkling wine, for example [8]. Furthermore, these two scaling laws enable us to untangle the intricate role of viscosity in the end-pinching mechanism by defining exactly at which step of the bubble bursting process it influences the drop size selection. Indeed, viscosity appears in Eq. (2) and not in Eq. (4), namely, when the drop size is expressed as a function of the bubble radius and not when it is expressed as a function of the jet velocity. Moreover, we know that, when a bubble collapses, it generates a jet whose velocity is selected by various ingredients including viscosity [inset of Fig. 3(a)] [3]. Therefore, viscosity appears in Eq. (2) because of its role in the jet velocity selection and, once the jet is rising, viscosity does not play an active role anymore, in particular in the drop detachment, and stays hidden in the jet velocity in Eq. (4). This implies that, once the jet velocity and shape are given, inviscid considerations would properly describe the drop detachment. Finally, contrary to the liquid viscosity, which does not participate to the drop detachment process itself (Mo $\lesssim 10^{-8}$), the duet gravity-capillarity seems to initiate the drop detachment by balancing the jet inertia and pulling on the jet tip. Our results probably do not apply to inertial stretched jets other than those created by bubble bursting, as the intrinsic jet shape and size are hidden in the scaling law. However, these results would need to be compared to the top breakup of other kinds of stretched jets (cavity collapse after impact, bubble pinch-off, etc.).

The Direction Générale de l'Armement is acknowledged for its financial support.

[1] F. Veron, Ocean spray, Annu. Rev. Fluid Mech. **47**, 507 (2015).
[2] H. Lhuissier and E. Villermaux, Bursting bubble aerosols, J. Fluid Mech. **696**, 5 (2012).
[3] E. Ghabache, A. Antkowiak, C. Josserand, and T. Séon, On the physics of fizziness: How bubble bursting controls droplets ejection, Phys. Fluids **26**, 121701 (2014).
[4] G. de Leeuw, E. L. Andreas, M. D. Anguelova, C. W. Fairall, E. R. Lewis, C. O'Dowd, M. Schulz, and S. E. Schwartz, Production flux of sea spray aerosol, Rev. Geophys. **49**, 05 (2011).
[5] E. R. Lewis and S. E. Schwartz, *Sea Salt Aerosol Production: Mechanisms, Methods, Measurements and Models*, Geophysical Monograph Series Vol. 152 (American Geophysical Union, Washington, DC, 2004).

[6] G. Liger-Belair, G. Polidori, and P. Jeandet, Recent advances in the science of champagne bubbles, Chem. Soc. Rev. **37**, 2490 (2008).
[7] E. Ghabache, G. Liger-Belair, A. Antkowiak, and T. Séon, Evaporation of droplets in a champagne wine aerosol, Sci. Rep. **6**, 25148 (2016).
[8] E. Ghabache, Surface libre hors équilibre: De l'effondrement de cavité aux jets étirés, Ph.D. thesis, UPMC, 2015, https://tel.archives-ouvertes.fr/tel-01292582.
[9] D. E. Spiel, The number and size of jet drops produced by air bubbles bursting on a fresh water surface, J. Geophys. Res. **99**, 10289 (1994).
[10] J. B. Keller, A. King, and L. Ting, Blob formation, Phys. Fluids **7**, 226 (1995).
[11] H. A. Stone and L. G. Leal, Relaxation and breakup of an initially extended drop in an otherwise quiescent fluid, J. Fluid Mech. **198**, 399 (1989).
[12] A. A. Castrejón-Pita, J. R. Castrejon-Pita, and I. M. Hutchings, Breakup of Liquid Filaments, Phys. Rev. Lett. **108**, 074506 (2012).
[13] M. Singh, H. M. Haverinen, P. Dhagat, and G. E. Jabbour, Inkjet printing-process and its applications, Adv. Mater. **22**, 673 (2010).
[14] J. M. Gordillo and S. Gekle, Generation and breakup of Worthington jets after cavity collapse. Part 2. Tip breakup of stretched jets, J. Fluid Mech. **663**, 331 (2010).
[15] T. Séon and A. Antkowiak, Large Bubble Rupture Sparks Fast Liquid Jet, Phys. Rev. Lett. **109**, 014501 (2012).
[16] E. Ghabache, T. Séon, and A. Antkowiak, Liquid jet eruption from hollow relaxation, J. Fluid Mech. **761**, 206 (2014).
[17] P. L. L. Walls, L. Henaux, and J. C. Bird, Jet drops from bursting bubbles: How gravity and viscosity couple to inhibit droplet production, Phys. Rev. E **92**, 021002 (2015).
[18] C. F. Kientzler, A. B. Arons, D. C. Blanchard, and A. H. Woodcock, Photographic investigation of the projection of droplets by bubbles bursting at a water surface1, Tellus **6**, 1 (1954).
[19] S. R. Massel, *Ocean Waves Breaking and Marine Aerosol Fluxes* (Springer, Berlin, 2007).
[20] G. B Deane and M. D. Stokes, Scale dependence of bubble creation mechanisms in breaking waves, Nature (London) **418**, 839 (2002).
[21] G. Liger-Belair, A. Conreux, S. Villaume, and C. Cilindre, Monitoring the losses of dissolved carbon dioxide from laser-etched champagne glasses, Food Res. Int. **54**, 516 (2013).